NJC

ROYAL SOCIETY OF CHEMISTRY

PAPER

View Article Online
View Journal | View Issue

Cite this: *New J. Chem.*, 2024, **48**, 5278

Preparation of stable Fe_2O_3/Ag nanocomposite particles with catalytic, antioxidant and antibacterial properties†

M. Ahasanur Rabbi, *[a] Most. Bithi Akter,[b] Bijan Mohon Chaki,[b] Md. Abdul Latif,[b] Md. Al-Amin,[a] M. Zia Uddin Rasel,[a] Shamsad Sharmin,[a] Md. Abdurrahim,[c] Mirza Humaun Kabir Rubel[d] and Md. Rowshanul Habib[e]

Nanomaterials have demonstrated a wide range of applications and amongst nanomaterials, most of the research has mainly focused on nanoparticles as they can be easily prepared and manipulated. The magnetic properties of certain magnetic nanoparticles have attracted a lot of interest in environmental applications. However, because of their great vulnerability to chemical and physical activity, their magnetic characteristics deteriorate. These nanoparticles are being progressively attempted to be encapsulated by a green organic matrix, which greatly improves usefulness, stability, and affordability, and reduces back toxicity. In this investigation, iron oxide (IO) nanoparticles were prepared by a co-precipitation method and these bear IO particles were stabilized by green synthesized silver nanoparticles to produce IO/Ag nanocomposite particles. The nano size of the prepared particles was confirmed by FE-SEM and TEM analysis. Incorporation of silver nanoparticles (AgNPs) on IO particles was confirmed by UV-Vis, XRD, TGA, and VSM. The improved stability of the magnetic particles was confirmed by DLS and zeta potential. Using the reducing agent $NaBH_4$, the catalytic reduction ability of the IO/Ag nanocomposite particles is investigated in relation to the degradation of Congo Red, a model anionic azo dye. When 40 μg mL^{-1} of IO/Ag particles were used, complete degradation of 20 mL of CR (0.1 mM) dye solution was accomplished in 2 minutes. The particles also demonstrated moderate antibacterial activity against four pathogens and good DPPH free radical scavenging activity, with 94% scavenging recorded at a concentration of 100 μg mL^{-1} particles.

Received 27th December 2023,
Accepted 19th February 2024

DOI: 10.1039/d3nj05885a

rsc.li/njc

1. Introduction

Composite materials are formed by the combination of two or more different materials or elements with different properties. Within the composite the constituent materials do not dissolve or blend into each other; therefore, the distinctive constituents can be identified separately.[1] When two or more constituents are merged, the properties of the composite differ from those of its separate constituents. Multi-phasic composite materials' exceptional structural and non-structural qualities have led to an expansion in their industrial uses; as a result, research in this area is linked to the ongoing creation of novel composite materials.[2] With the advancement of nanotechnology, researchers have widely used various nanofillers in their research to improve the performance of composite materials and multi-phasic materials in which at least one of the phases shows dimensions in the size range below 100 nm are known as nanocomposites.[3,4] With the exponential growth of nanotechnology, nanocomposites are receiving a lot of attention from both academic and industrial researchers. They combine the properties of the filler with the matrix material to produce novel functional materials that are customized to meet the demands of a particular use. Generally speaking, nanohybrids employ a broad range of host materials, including silica, organic polymers, and even liquid media. Particularly interesting are host materials with adjustable characteristics that change in response to an external stimulus, such as pH,[5,6] temperature,[7,8] magnetic fields,[9–11] electric fields[12] and mechanical stress.[13] In recent times, composite materials have been developed from components such as polymer

[a] *BCSIR Rajshahi Laboratories, Bangladesh Council of Scientific and Industrial Research (BCSIR), Rajshahi-6206, Bangladesh. E-mail: rabbi_chem@yahoo.com*
[b] *Department of Chemistry, Begum Rokeya University, Rangpur-5404, Bangladesh*
[c] *Biomedical and Toxicological Research Institute, Bangladesh Council of Scientific and Industrial Research (BCSIR), Dhaka 1205, Bangladesh*
[d] *Department of Material Science & Engineering, Rajshahi University, Rajshahi 6205, Bangladesh*
[e] *Department of Biochemistry and Molecular Biology, Rajshahi University, Rajshahi 6205, Bangladesh*

† Electronic supplementary information (ESI) available. See DOI: https://doi.org/10.1039/d3nj05885a

matrix,[14] ceramic matrix,[15] and metal matrix.[9] The inclusion of nanoparticles into various materials may be customized to achieve specific features, and these materials have demonstrated considerable potential for certain applications.[16–18] Magnetic nanocomposites are an important part of composite materials, and the design, synthesis, and production of magnetic composite materials are the subject of intensive study.[19] Due to their high saturation magnetization, biocompatibility, low toxicity, stability, ease of separation, cost-effectiveness, and signal detecting capabilities, magnetic nanocomposites have found extensive applications in a variety of fields.[20] The fundamental concept behind the creation of magnetic nanocomposites is the combination of magnetic characteristics and unique qualities for specific objectives.[21] Comparing iron oxide-based nanocomposites to other transition metal oxides containing divalent ions such as Cu(II), Cd(II), Mn(II), Ni(II), and Zn(II), they are safer for the environment. Nanocomposites have excelled in adsorption, photocatalysis, catalysis, sensing, and biosensor applications in environmental applications. The strengths for the adsorption and catalysis sector are particularly the facile separation due to the magnetically recoverable nano catalyst.[22] Additionally, the creation of an iron oxide nanocomposite with high stability is still a difficult problem, particularly for biomedical applications. So far, iron oxide nanoparticles and iron oxide-based materials have been prepared by hydrothermal,[23,24] co-precipitation,[9,25,26] sonochemical,[27,28] laser pyrolysis,[29,30] and electrochemical deposition methods.[31,32] Different magnetic nanoparticles may be created by generating unique morphologies, depending on the synthesis process and factors such as temperature, pressure, reaction time, reagent casting, *etc.* Pure magnetic nanoparticles like to aggregate, regardless of the synthesis pathway, which limits their area and dispersion capabilities. Furthermore, air exposure quickly oxidizes pure magnetic nanoparticles, causing a progressive loss of their magnetic properties.[33] Most scientists working on this topic are interested in improving the characteristics of magnetic composites, which are created when magnetic nanoparticles are combined with organic molecules or other stable nanoparticles. To prevent oxidation and agglomeration of magnetic nanoparticles, it is crucial to develop an effective protection method. To avoid aggregation, magnetic nanoparticles are grafted on or coated with surfactants, polymers or other organic species.[34] Stabilization can also be done with other stable metal or non-metal nanoparticles. In this stabilization process the naked magnetic nanoparticles are blended with another stable metal nanoparticle. Most of the time, protective approaches serve as a functionalization procedure in addition to stabilizing magnetic nanoparticles. The desired application guides the selection of these functionalization processes. Biolabeling, bioseparation, and catalysis are just a few of the uses for functionalized magnetic nanocomposites. Because of their great reactivity, excellent dispersion, and ease of separation, functionalized magnetic nanoparticles are very helpful in liquid-phase catalytic processes. From an industrial standpoint, magnetic separation is an economical and dependable method for separating nanoparticles or nanocomposites.[35,36] Considering the vast potentiality of magnetic nanocomposites, this work aims to apply *Bixa orellana* seed extract to synthesize and stabilize magnetic nanoparticles as well as magnetic nanocomposites.

2. Materials and methods

2.1 Materials

Seeds of *Bixa orellana* were gathered from a distant region in Rajshahi. In the research project, all compounds were of reagent grade purity. We bought ferrous sulfate and ferric chloride from Merck Life Science Limited in India. The following materials were acquired from Merck, Germany: ammonia solution, sodium hydroxide, silver nitrate, and 1,1-diphenyl-2-picrylhydrazyl (DPPH). Bacterial strains *Shigella boydii, Shigella dysenteriae, Staphylococcus aureus and Escherichia coli* were supplied by Rajshahi University's Department of Biochemistry and Molecular Biology.

2.1.1 Extraction of biomolecules. To extract the biomolecules 20 g *Bixa orellana* seed was taken in a 1000 mL beaker along with 200 mL of distilled water and 1 mL of a NaOH solution (1 M). Using a DLAB MS7-H550-S magnetic hot plate stirrer, the mixture was heated to 70 °C while being continuously stirred for 30 minutes. Using a clean muslin cloth to filter, the first extract was obtained. The beaker holding the seed residue was again filled with 200 mL of distilled water and a 1 M NaOH solution. It was then agitated for two hours at 70 °C. After collecting the second extract by filtration using a second muslin cloth, the filtrates from the two were combined. Prior to the synthesis of nanoparticles, the filtrate was lastly filtered once more using Whatmann filter paper and kept at 4 °C.

2.1.2 Preparation of magnetic nanoparticles (MNPs). The ironoxide (IO) nanoparticles were prepared by a slightly modified green synthesis process. Ferric (Fe^{3+}) and ferrous (Fe^{2+}) in an aqueous mixture were mixed at a 2 : 1 molar ratio to create iron oxide nanoparticles. Magnetic nanoparticles were made using the co-precipitation technique using 2.40 g ferric chloride ($FeCl_3{\cdot}6H_2O$) and 2.10 g ferrous sulfate ($FeSO_4{\cdot}7H_2O$). Two salts were dissolved in 300 mL water under magnetic stirring at 60 °C. After 10 minutes, about 25 mL *Bixa orellana* seed extract and 25 mL of 25% liq. NH_3 were added to the mixture while stirring. The reaction occurred at below 60 °C for 4 hours. After completion of the reaction, the product was cooled at room temperature. The supernatant was thrown away once the particles were separated by an external magnet, and the particles were then re-dispersed in deionized water. Until the pH of the supernatant reached neutral, this procedure was repeated.

2.1.3 Preparation of magnetic Fe_2O_3/Ag nanocomposites. Washed IO nanoparticles were re-dispersed in 100 mL of distilled deionized water by using a bath Sonicator for 30 minutes. Then, 100 mL of 0.01 M $AgNO_3$ solution was added to this dispersion and stirred for another 30 minutes. After that, 50 mL *Bixa orellana* seed extract along with 5 mL 1% NaOH was slowly added to the mixture of IO nanoparticles and silver nitrate under continuous stirring. The reaction was carried out with continuous mechanical stirring for 4 h at room

temperature. After completion of the reaction, the mixture was allowed to stand for 24 hours. The final black colored product was confirmed to be reduced Ag^+ ions. The black colored product was separated by applying an external magnetic field and washed five times with deionized water by magnetic decantation to remove any nonmagnetic by-products. The magnetic response of the prepared particles confirmed the formation of the IO/Ag nanocomposite.

2.2 Characterization

Seed extract and a dilute dispersion of prepared IO and IO/Ag particles were analyzed in spectrum scan mode at the wavelength range of 200 to 800 nm using a UV-visible spectrophotometer (SP-UV-500DB, Spectrum instrument, Germany). Ultra-high resolution scanning electron microscope (SEM) images were captured by a JSM-7610F (JEOL). Prior to SEM imaging, the samples underwent platinum coating with a JEOL Auto fine coater (JEC-3000FC). SEM photographs of IO and IO/Ag particles were captured at a magnification of ×200 K and operating voltage range of 5 to 15 kV. The EDX spectrum was recorded using an energy dispersive X-ray spectroscopy adaptor that was attached to the SEM. The thermal characteristics of 10.0 mg of dry powder samples were measured using a thermogravimetric analyzer (TGA, STA 8000, PerkinElmer, Netherlands). Under a flowing nitrogen atmosphere, the mass loss in percentages was recorded with 10.0 mg of dry powder samples at a heating rate of 20 °C min^{-1}. FTIR analysis was performed by a PerkinElmer's FTIR-1400 (United Kingdom). Dried samples of *Bixa orellana* seed extract, IO nanoparticles and the IO/Ag nanocomposite were scanned covering the range of 4000 to 400 cm^{-1} with an average 20 scans. TEM images captured using a Thermofisher Scientific's Taalos F 200X transmission electron microscope were used to describe the shape and size of the produced IO and IO/Ag particles. The TEM measurement was carried out by applying a drop of colloidal dispersion to a 300-mesh copper (Cu) grid that had been coated with carbon film, and letting the solvent evaporate in the air at ambient temperature. Using a particle size analyzer, the size distributions and zeta potential of the produced particles were examined. Using a Horiba analyzer (SZ-100), the colloidal dispersion of the IO and IO/Ag particles was examined. Dynamic light scattering (DLS) at 25 °C and a scattering angle of 90 is used to analyze particle size. The X-ray diffraction (XRD) patterns of the synthesized particles were recorded using a scanning X-ray diffractometer (Bruker D8 Advance, Germany), with the intensity measurements being done at 2θ values ranging from 10 to 80°. Here, a position-sensitive detector aperture operating at 25 °C was used with a scanning rate of 1° min^{-1}. The diffraction spectrum was processed using semi-quantitative phase analysis software, which helped to reduce noise, smooth the data, and pinpoint the peaks. A vibrating sample magnetometer (VSM, Model DXV-100, China) was used to measure the magnetic properties.

2.3 Catalytic activity

The catalytic activity of IO/Ag was investigated according to Rabbi *et al.* (2021).[9] Congo Red (CR) dye in an aqueous solution deteriorated in the presence of IO/Ag and $NaBH_4$. A mixture of 2.0 mL of 1 M $NaBH_4$ and 18 mL of 0.1 mM CR dye was created. Using particles at 10, 20, 30 and 40 μg mL^{-1}, the catalytic activity of the IO/Ag nanocomposite was assessed. Absorbance at a fixed wavelength of 500 nm was recorded to monitor the time-dependent decline in CR content in aqueous solution. Without any catalysts to act as a control, the experiment was conducted again.

2.4 Antioxidant assay

The DPPH assay method, as previously reported by[37] Shen *et al.* (2010), was utilized in this study to assess the IO/Ag nanocomposite particles' potential to scavenge free radicals. First, a 0.1 mM DPPH solution was made in methanol for the experiment. Subsequently, 3 mL of methanolic dispersion of synthesized IO/Ag was mixed with 1 mL of this solution. The DPPH scavenging activity was investigated with varying particle concentrations (40, 60, 80 and 100 μg mL^{-1}) and ascorbic acid was utilized as a reference material. The mixes were given a thorough shake and then left for 30 minutes at room temperature in a dark area. The proportion of DPPH radical scavenging was then computed using the following formula after the absorbance at 517 nm was measured. The following formula was used to determine the capacity to scavenge the DPPH radical.

$$\text{DPPH scavenging effect (\% inhibition)} = \{((A_0 - A_1)/A_0) \times 100\}$$

where A_0 is the absorbance of the control reaction, and A_1 is the absorbance in the presence of the samples and reference. All the tests were performed in triplicate and the results were averaged.

2.5 Antibacterial assay

The antibacterial efficacy of the synthesized IO/Ag was evaluated by using the disc diffusion test technique.[38] Solid nutrition agar medium was poured into each sterile Petri dish, and the cultured pathogens (0.2 mL) were placed on top. Subsequently, the growing test organism was carefully covered with filter paper disks at three separate locations and a standard erythromycin disc served as a positive control in the individual Petri dishes. A micropipette was then used to gently drop a dispersion having three different concentrations (35, 70, and 105 μg $disc^{-1}$) of IO/Ag particles over each disc. These antibacterial test plates were incubated for twenty-four hours at 37 ± 1 °C to confirm bacterial growth, after four hours of sample diffusion at 4 °C in the refrigerator. Every experiment was conducted in triplicate, and the width of the zone of inhibition encircling each filter paper disc was measured.

3. Results and discussion

Formation of ironoxide (IO) nanoparticles by the co-precipitation method was confirmed by the color change of the reaction mixture[39] and also by the external magnetic field [Fig. 1(a)]. The IO/Ag nanocomposites are also produced by the intense color change [Fig. 1(c)].

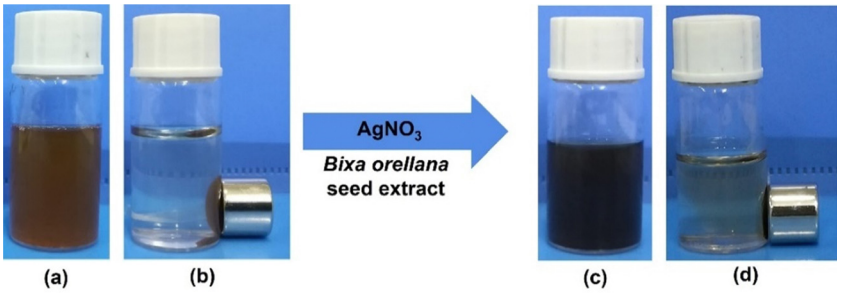

Fig. 1 (a) IO nanoparticles dispersed in water, (b) IO separated by an external magnetic field, (c) the IO/Ag nanocomposite dispersed in water and (d) the IO/Ag nanocomposite separated by an external magnetic field.

3.1 Characterization

Fig. 2 shows the UV-Vis spectra of (a) ironoxide nanoparticles, (b) *Bixa orellana* seed extract and (c) the ironoxide/Ag nanocomposite. The absorption maximum for the seed extract was observed at 275 nm, which is common to all phenolic substances. The composite particle IO/Ag nanocomposite showed the characteristic surface plasma resonance (SPR) of silver nanoparticles. SPR absorption at 410 nm confirmed the formation of the magnetic silver nanocomposite.[9]

To comprehend the nanoparticles' crystalline structure, X-ray diffraction (XRD) was used. Usually in powdered form, the sample consisted of tiny grains of crystalline substance to be investigated.[40] The XRD pattern of the IO nanoparticles and IO/Ag nanocomposites is shown in Fig. 3. Sharp peaks of IO and IO/Ag are attributed to the highly crystalline nature of the particles. The diffraction peaks for the IO nanoparticles were seen at 2θ values of around 30.5, 35.82, 43.7, 57.66, and 63.2. These values may correspond to the crystal planes (220), (311), (400), (333), and (440).[41] The magnetite standard XRD pattern (card JCPDS #89-4319) and the observed XRD pattern agreed well. Furthermore, the pattern indicated that the bulk of the particles had a faced-centered cubic (FCC) crystalline structure. The diffraction pattern of the IO/Ag nanocomposite particles [Fig. 3(b)] further verified that composite particles were crystalline in nature. New diffraction signals appear at 38.4°, 44.54°, 57.76°, and 77.94° for the composite particles. These signals represent the (111), (200), (220), and (311) reflection plane of the silver nanoparticles.[42] During the formation of the IO/Ag nanocomposite particles, silver might be deposited on the surface of the iron oxide particles. For this reason, in the XRD pattern of the IO/Ag nanocomposite particles, the diffraction signals due to iron oxide seed particles almost disappeared.

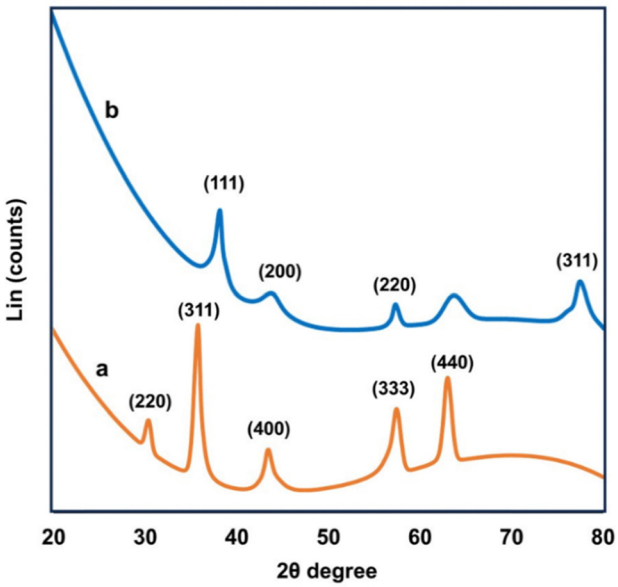

Fig. 3 (a) XRD patterns of (a) IO nanoparticles and (b) the IO/Ag nanocomposite.

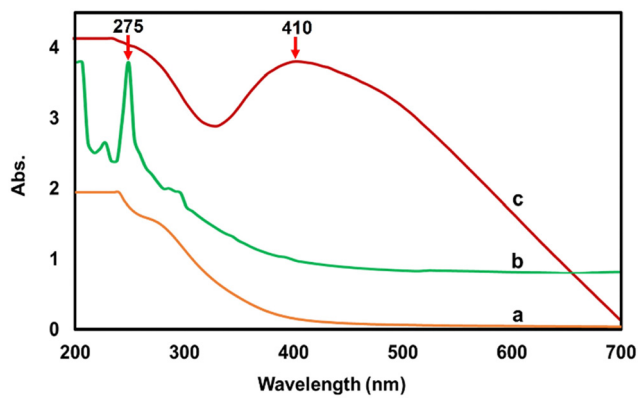

Fig. 2 UV-Vis spectra of (a) IO, (b) *Bixa orellana* seed extract, and (c) the IO/Ag nanocomposite.

The morphology and size of the prepared ironoxide (IO) nanoparticles and ironoxide/silver (IO/Ag) nanocomposite particles was studied using FE-SEM. The formation of spherical shaped IO nanoparticles and the IO/Ag nanocomposite can be observed from the FE-SEM images (Fig. 4). Both the IO nanoparticles and IO/Ag nanocomposites are agglomerated, but still high-resolution images from the upper-most surface of a specimen showed the monodisperse nano sized particles. Agglomeration occurs during the drying process of the nanosuspensions into dry powders.[43] In the FE-SEM images of IO and IO/Ag, relatively lower agglomeration was observed in the composite than the iron oxide particles, suggesting that the composite is more stable than bare iron oxide.

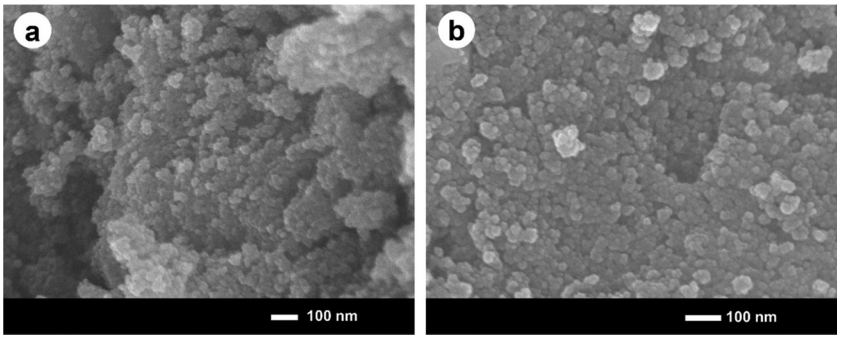

Fig. 4 SEM images of (a) IO nanoparticles and (b) the IO/Ag nanocomposite.

An accurate understanding of the elements included in the biosynthesized nanoparticles may be obtained from the EDX result. As seen in Fig. 5(a), the EDX profile of IO reveals a strong signal from the Fe atom, indicating the crystalline characteristics. The horizontal axis shows energy in keV, while the vertical axis shows the total number of X-ray counts. As is common for the absorption of metallic iron nanocrystallites, the main absorption peak is located at 6.38 keV.[44] In the EDX spectrum of the IO/Ag nanocomposites [Fig. 5(b)], a prominent absorption peak was observed at 2.98 keV for silver together with the metallic iron nanocrystallites. The atom percentages of iron and silver were found to be 36.64 and 12.66%, respectively. In addition to these signs for C, O signals are also seen, which might come from the *Bixa orellana* seed extract.

The TEM pictures (Fig. 6 and 7) verified the intricate morphology and nanoscale dimensions of the IO nanoparticles and IO/Ag nanocomposites. The individual particles' spherical-like form, ranging in size up to 20 nm, is characteristic of magnetic nanoparticles produced by co-precipitation.[45,46] The IO nanoparticle's crystalline character was shown by the SAED data [Fig. 6(c)]. A lower magnification picture shows that the IO nanoparticles and IO/Ag nanocomposites are embedded in a thick matrix, which might be the organic stabilizing agents (seed extract of *Bixa orellana*) used in the synthesis.[47] This showed unequivocally that the *Bixa orellana* seed aqueous extract was very suitable for lowering the amount of silver particles in the medium and converting them into evenly distributed IO/Ag nanocomposites. The crystalline nature of the IO/Ag nanocomposite was confirmed by SAED [Fig. 7(c)], which displayed a diffraction pattern of the nanocomposites directed toward the (111), (200), (220), and (311) crystalline planes. These planes match the face-centered cubic (FCC) structure of elemental silver.

TGA analysis was done to determine the thermal stability of the IO nanoparticles and IO/Ag nanocomposite. TGA measurements were performed with a heating rate of 10 C min^{-1} in the temperature range of 30 °C to 800 °C. The TGA curve of (a) the ironoxide nanoparticles and (b) ironoxide/silver nanocomposite is shown in Fig. 8. For pure IO nanoparticles no or slight weight loss due to absorbed moisture is expected.[48] In this case, IO nanoparticles were stabilized by *Bixa orellana* seed extract, which results in gradual weight loss up to 360 °C. Up to 800 °C 6.75% weight loss can be explained due to evaporation of water and biomolecules. Whereas more weight loss for the IO/Ag nanocomposite can be explained by the incorporation of more biomolecules as a stabilizing agent of silver particles.[49] The residual weight percentage of IO/Ag nanocomposite was found to be 89.40%.

A vibrating sample magnetometer was used to test the magnetic properties of the magnetic particles.[50] The hysteresis loops of the bare IO nanoparticles and IO/Ag nanocomposites are shown in Fig. 9. A material's maximal magnetic response in an external magnetic field is known as saturation magnetization (Ms), and it is used to quantify the magnetic characteristics. The saturation magnetizations of the bare IO nanoparticles and IO/Ag nanocomposites are 32.3 emu g^{-1}

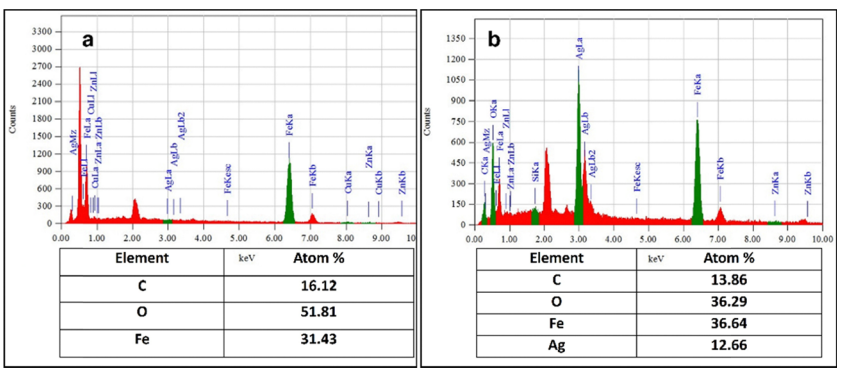

Fig. 5 EDX spectra with the atom% of (a) IO nanoparticles and (b) the IO/Ag nanocomposite.

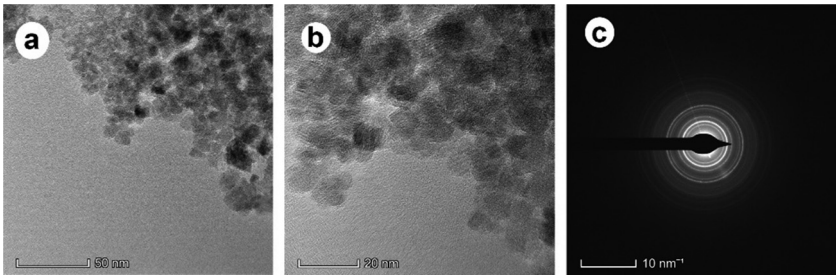

Fig. 6 TEM images of IO nanoparticles at (a) low magnification, (b) high magnification and (c) SAED.

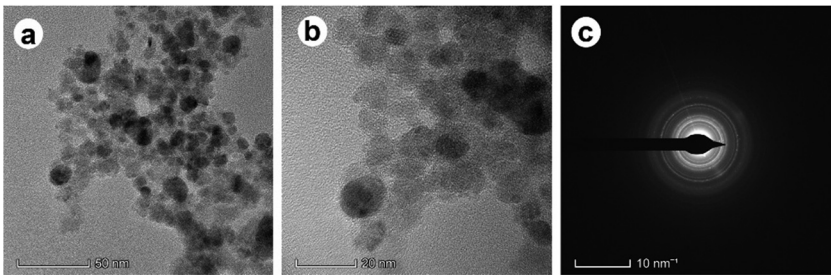

Fig. 7 TEM images of the IO/Ag nanocomposite at (a) low magnification, (b) high magnification and (c) SAED.

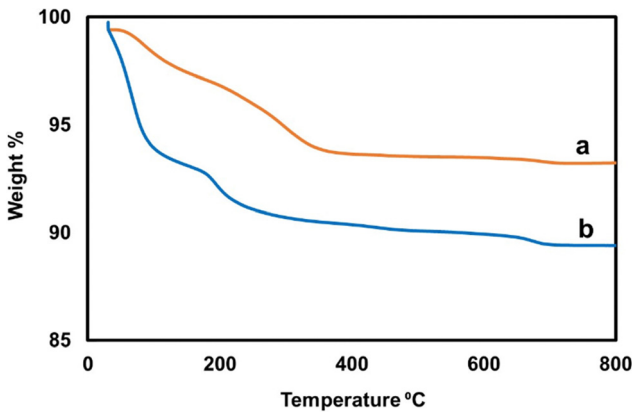

Fig. 8 TGA Thermographs of (a) IO nanoparticles and (b) the IO/Ag nanocomposite.

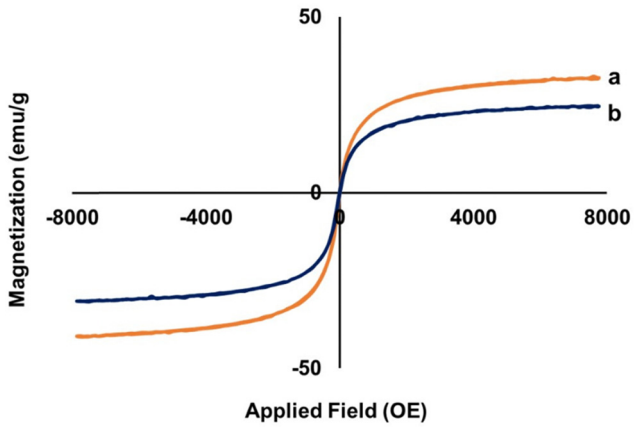

Fig. 9 Hysteresis loops (VSM) of (a) IO nanoparticles and (b) the IO/Ag nanocomposite.

and 24.4 emu g^{-1} respectively. Inclusion of nonmagnetic silver nanoparticles reduces the Ms value of the IO/Ag nanocomposite particles. The magnetization drops from a plateau condition to zero when the magnetic field is removed from both particles. This action and the 'S' type reversible magnetization curve confirmed the paramagnetic property of the particles.[9,26] These findings indicate that our synthesized IO nanoparticles and IO/Ag nanocomposites exhibit a suitable magnetic behavior and can be easily separated from waste-water treatment plants after their application as a catalyst.

The biomolecules involved in the stabilization of IO nanoparticles and the IO/Ag nanocomposite were identified and characterized by FTIR spectroscopy. Fig. 10 displays the FTIR spectra of the IO nanoparticles, IO/Ag nanocomposite, and seed extract of *Bixa orellana*. The seed extract showed the absorption bands at 2973, 1568.1, 1380.71, and 1065.23 cm^{-1} corresponding to the C–H stretching, C–C stretching and C–H bending and C–O (alcohol) stretching vibrations, respectively.[51–54] With the exception of a little shift in peak location and intensity, the FTIR spectra of AgNPs and the seed extract exhibited remarkable resemblance.[55] FTIR examination of the produced IO and IO/Ag verified the seed extract's dual function as a capping and reducing agent as well as the existence of the identical functional groups within both particles. In the spectra of IO and IO/Ag, the wide bands for the stretching vibrations of O–H (alcohol/phenol) at 3600–3200 cm^{-1} were reduced. The hydroxyl group's role in the creation and stability of iron oxide

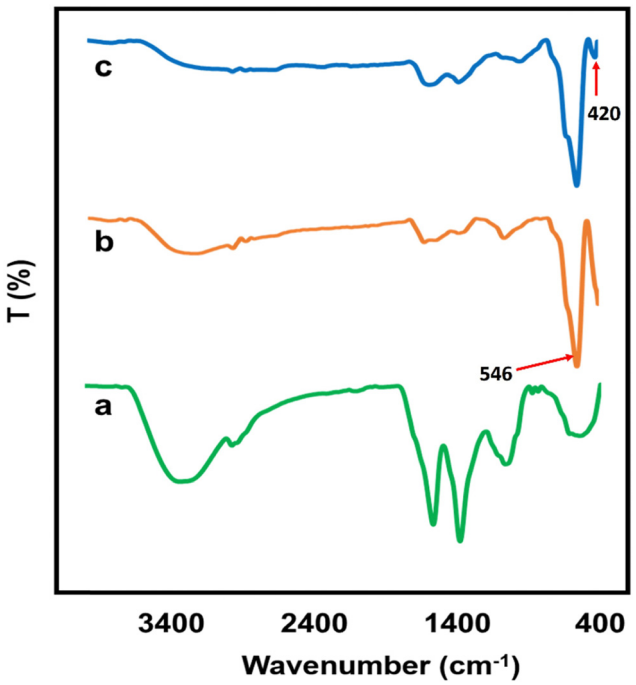

Fig. 10 FTIR spectra of (a) *Bixa orellana* seed extract, (b) IO nanoparticles and (c) the IO/Ag nanocomposite.

and the iron oxide/silver nanocomposite is responsible for the diminished O–H stretching vibrations.[56] For the Fe–O group vibration, an intense peak at wave number 546 cm^{-1} may have formed. The Ag–O may be represented as the shoulder peak in the IO/Ag FTIR spectrum at 417 cm^{-1}.

The DLS histogram (Fig. 11) was used to calculate the average hydrodynamic diameters of the IO nanoparticles and the IO/Ag colloidal dispersion. It was discovered that the IO and IO/Ag had hydrodynamic diameters of 697.1 and 531.1 nm, respectively. IO and IO/Ag have polydispersity indices (PIs) of 0.405 and 0.408, respectively. According to Liz-Marzan *et al.* (1996),[57] the colloidal dispersions of IO and IO/Ag were monodispersed in nature if the PI of both particles was less than 0.5. DLS measures the diameter of the particles as they disperse in liquid rather than the actual size of the nanoparticles. As a consequence, the DLS values for the biosynthesized IO and IO/Ag in this work are bigger than the SEM and TEM results. The study[58–60] claims that Brownian motion is the cause of the size discrepancy between DLS, SEM, and TEM. A decrease in hydrodynamic diameter during IO/Ag nanocomposite production can be attributed to the composite's increased stability and decreased quantity of aggregation.

Zeta potential is significant because it has a relationship with the short- and long-term stability of dispersion. While emulsions with low zeta potentials tend to flocculate or coagulate, potentially resulting in poor physical stability, dispersions with high zeta potentials—whether positive or negative—are electrically stabilized. Generally, nanoparticles with a high zeta potential have more repulsive forces than attractive forces, which leads to a more stable system.[61,62] The zeta potential value (Fig. 12) of IO and IO/Ag also supports the increased stability of the prepared nanocomposite. The zeta potential of bear IO nanoparticles was −35.7 mV, whereas the value increased to −46.4 mV for the IO/Ag nanocomposite.

3.2 Catalytic activity

This study examined the dye degradation potential of the IO/Ag nanocomposite in the presence of sodium borohydride ($NaBH_4$). Congo Red (CR) dye was eliminated from the water medium by catalytic reduction. Different concentrations of IO/Ag nanocomposite particles (10, 20 and 30 μg mL^{-1}) were used in this experiment. After the addition of the IO/Ag catalyst, degradation of the dye was visually observed within a few minutes by the change of deep red color, which was further confirmed by the decrease in absorbance value. Similar to any other catalyst system, the degradation rate increases with catalyst concentration. In the presence of 10, 20, 30 and 40 μg mL^{-1} particles, the azo dye totally decomposed in 8, 7, 5 and 2 minutes, respectively (Fig. 13). According to the earlier work, the presence of silver nanoparticles on the surface of the IO/Ag composite particles might account for this rapid deterioration.[56]

3.3 Antioxidant & antibacterial activity

By using the DPPH radical scavenging experiment, the antioxidant properties of the IO/Ag nanocomposite particles were examined and contrasted with ascorbic acid standard (Fig. 14). Researchers found that when compared to plant extract alone, AgNPs and their nanocomposites made using a green reaction strategy have better antioxidant activity.[63–65] Although DPPH is a persistent free radical at ambient temperature, it may be decreased by accepting hydrogen in the presence of an

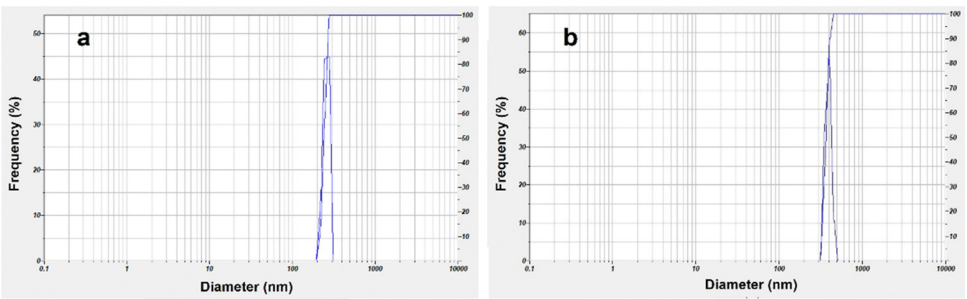

Fig. 11 Size distribution of (a) IO and (b) IO/Ag particles as studied by DLS.

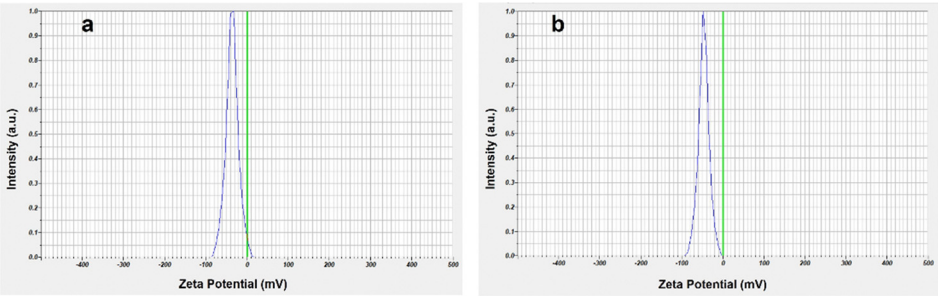

Fig. 12 Zeta potential measurements of (a) IO and (b) IO/Ag particles.

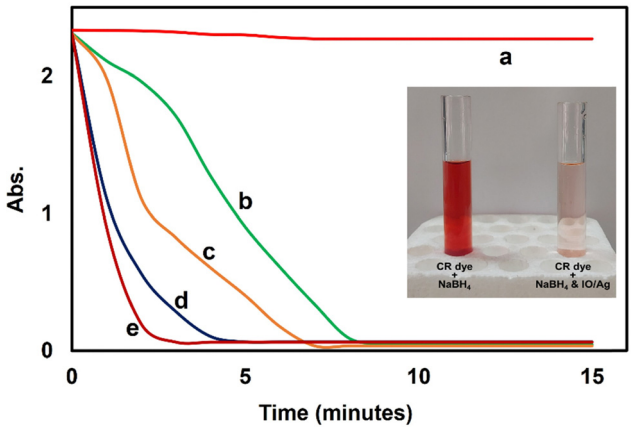

Fig. 13 Reductive degradation of 0.1 mM CR in the presence of (a) no catalyst, (b) 10 μg mL^{-1}, (c) 20 μg mL^{-1}, (d) 30 μg mL^{-1} and (e) 40 μg mL^{-1} IO/Ag particles.

antioxidant molecule, producing a colorless methanol solution.[9] According to previously published literature, the bear IO nanoparticles didn't exhibit antioxidant activity. The IO/Ag nanocomposite particles' ability to scavenge free radicals grows progressively as the particle concentration rises, maximum activity was found at around 94% when the dispersion contains 100 μg mL^{-1} of particles. According to this investigation, the produced IO/Ag nanocomposite particles have free radical scavenging ability that is comparable with the standard ascorbic acid. As a result, the produced nanocomposite particles may be helpful in the treatment of several oxidative stress-related illnesses.

3.4 Antibacterial activity assay

Antibacterial nanocomposite particles offer a wide range of potential applications in the biomedical area and in many everyday health goods.[66,67,68] Four pathogens have been examined in relation to the antibacterial properties of IO/Ag nanocomposite particles (Fig. 15). Gram positive (*Staphylococcus aureus*) and Gram negative (*Escherichia coli*, *Shigella dysenteriae, and Shigella boydii*) bacteria are both significantly inhibited by IO/Ag nanocomposite particles. As is typical for bacterially active particles, the antibacterial activity rises as the concentration of the particle increases. The inhibition zones in the presence of IO/Ag nanocomposite particles range from 07 to 12.5 mm, regardless of the kind of bacteria (Fig. S-1, ESI†). When *Staphylococcus aureus* is exposed to 105 μg $disc^{-1}$ of IO/Ag nanocomposite particles, a maximal inhibitory zone of 12.5 mm is seen. The bear IO nanoparticles didn't show any antibacterial effect, and thus the addition of AgNPs is responsible for the antibacterial activity of the IO/Ag nanocomposite particles. For IO/Ag nanocomposite particles, two possible antibacterial processes have been used. One is the release of Ag ions from AgNPs that penetrated the bacterial membrane and impacted respiration and osmosis. According to Agnihotri *et al.* (2013), the other is the contact killing mode that is often seen with anchored AgNPs.[69] According to the study mentioned

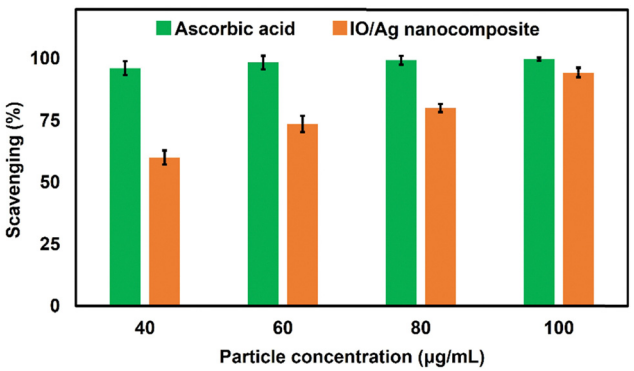

Fig. 14 Free radical scavenging activity of ascorbic acid and IO/Ag nanocomposite particles.

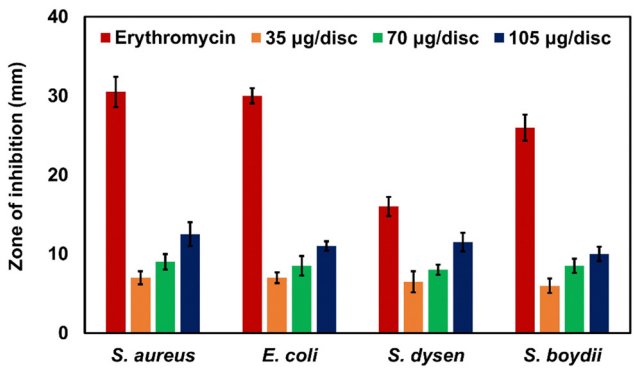

Fig. 15 Antibacterial activity of IO/Ag nanocomposite particles.

above, biocompatible and relatively less toxic IO/Ag nanocomposite particles with moderate antimicrobial activity will make promising bioactive nanomaterials because they can be readily recovered from application media, limiting the potential harm they could cause to the environment and human health.

4. Conclusions

In the present study, we have demonstrated the preparation of stable magnetic nanocomposite particles with moderate antioxidant and antibacterial activities. The biomolecules extracted from *Bixa orellana* seed were used to stabilize the bear magnetic nanoparticles as well as IO/Ag nanocomposite particles. Without any external stabilizer, the dispersions of both particles were stable; however, the IO/Ag particles were found to be more stable than the bear IO nanoparticles. It is plausible to presume that bear IO nanoparticles are largely coated with AgNPs based on the IO/Ag nanocomposite particle preparation technique. The IO/Ag nanocomposite particles' decreased saturation magnetization value further supported this. The nanocomposite particles maintained enough paramagnetic properties to allow for media separation even if their saturation magnetization decreased. We may conclude that the presence of nanosized silver particles on the surface of the nanocomposite is mostly responsible for the catalytic, antioxidant and antibacterial characteristics of the nanocomposite particles. Researchers are searching for smart particles that can be collected or separated from the environment after usage in order to address the environmental problem related to nanoparticles. In this regard, combining magnetic IO nanoparticles with AgNPs without changing their unique characteristics might be a good substitute.

Author contributions

M. Ahasanur Rabbi: investigation, methodology, data acquisitions, analyses writing original draft of the manuscript, reviewing and editing of the final manuscript. Most. Bithi Akter: conducting formal experiments, analyses, and data acquisitions; Bijan Mohon Chaki: supervision and validation of cured data; Md. Abdul Latif: project monitoring; Md. Al-Amin and M. Zia Uddin Rasel: supervision and validation of cured data; Shamsad Sharmin: review & editing; Md. Abdurrahim and Mirza Humaun Rubel: instrumental analyses; M. Rowshanul Habib: antibacterial assay.

Conflicts of interest

The authors confirm that they have no conflicts of interest and the data included in this manuscript have not been published previously.

Acknowledgements

This work was supported by the Bangladesh Council of Scientific and Industrial Research.

References

1 M. K. Egbo, *J. King Saud Univ. Eng. Sci.*, 2021, **33**, 557–568, DOI: 10.1016/j.jksues.2020.07.007.
2 A. Ali and A. Andriyana, *RSC Adv.*, 2020, **10**, 16390–16403, DOI: 10.1039/C9RA10594H.
3 M. S. S. Kumar, C. P. Selvan, K. Santhanam, A. Kadirvel, V. Chandraprabu and L. SampathKumar, *Adv. Mater. Sci. Eng.*, 2022, 2165855, DOI: 10.1155/2022/2165855.
4 S. H. Din, M. A. Shah, N. A. Sheikh and M. M. Butt, *Charact. Appl. Nanomater*, 2019, **3**, 875, DOI: 10.24294/can.v3i1.875.
5 Z. Zhang, C. J. R. Wells, A. M. King, J. C. Bear, G. Davies and G. R. Williams, *J. Mater. Chem. B*, 2020, **8**, 7264–7274, DOI: 10.1039/D0TB01033B.
6 M. A. Alam, M. A. Rabbi, M. A. J. Miah, M. M. Rahman, M. A. Rahman and H. Ahmad, *J. Colloid Sci. Biotechnol.*, 2012, **1**, 225–234.
7 D. Khedri, A. H. Hassani, E. Moniri, H. A. Panahi and M. Khaleghian, *Environ. Sci. Pollut. Res.*, 2023, **30**, 2494–2508, DOI: 10.1007/s11356-022-22389-y.
8 F. D. Jochum and P. Theato, *Chem. Soc. Rev.*, 2013, **42**, 7468–7483.
9 M. A. Rabbi, M. M. Rahman, H. Minami, N. Yamashita, M. R. Habib and H. Ahmad, *Carbohydr. Polym.*, 2021, **251**, 117024, DOI: 10.1016/j.carbpol.2020.117024.
10 R. Tognato, A. R. Armiento, V. Bonfrate, R. Levato, J. Malda, M. Alini, D. Eglin, G. Giancane and T. Serra, *Adv. Funct. Mater.*, 2019, **29**, 1804647, DOI: 10.1002/adfm.201804647.
11 J. Thevenot, H. Oliveira, O. Sandre and S. Lecommandoux, *Chem. Soc. Rev.*, 2013, **42**, 7099–7116.
12 T. Manouras and M. Vamvakaki, *Polym. Chem.*, 2017, **8**, 74–96.
13 D. A. Davis, A. Hamilton, J. Yang, L. D. Cremar, D. Van Gough, S. L. Potisek, M. T. Ong, P. V. Braun, T. J. Martínez, S. R. White, J. S. Moore and N. R. Sottos, *Nature*, 2009, **459**, 68–72.
14 M. A. Rabbi, M. M. Rahman, H. Minami, M. A. Rahman, S. M. Hoque and H. Ahmad, *Cellulose*, 2019, **26**(16), 8713–8727, DOI: 10.1007/s10570-019-02706-4.
15 S. Dhanasekar, A. T. Ganesan, T. L. Rani, V. K. Vinjamuri, M. N. Rao, E. Shankar, Dharamvir, P. S. Kumar and W. M. Golie, *Adv. Mater. Sci. Eng.*, 2022, **6160591**, 1–9, DOI: 10.1155/2022/6160591.
16 I. D. Ibrahim, T. Jamiru, E. R. Sadiku, Y. Hamam, Y. Alayli and A. A. Eze, *IET Nanodielectrics*, 2019, **2**(4), 115–122, DOI: 10.1049/iet-nde.2019.0014.
17 G. Yu, X. Xie, L. Pan, Z. Bao and Y. Cui, *Nano Energy*, 2013, **2**(2), 213–234, DOI: 10.1016/j.nanoen.2012.10.006.
18 Y. K. Sun, Z. Chen, H. J. Noh, D. J. Lee, H. G. Jung, Y. Ren, S. Wang, C. S. Yoon, S. T. Myung and K. Amine, *Nat. Mater.*, 2012, **11**, 942–947, DOI: 10.1038/nmat3435.
19 A. Walther and A. H. Müller, *Chem. Rev.*, 2013, **113**(7), 5194–5261, DOI: 10.1021/cr300089t.
20 A. Nisar, H. Zaman, M. Bilal, A. A. Shah, M. S. Nazir and H. M. N. Iqbal, *Sci. Total Environ.*, 2019, **670**, 523–538, DOI: 10.1016/j.scitotenv.2019.03.209.
21 M. I. A. Abdel Maksoud, R. A. Fahim, A. G. Bedir, A. I. Osman, M. M. Abouelela, G. S. EI- Sayyad,

M. A. Elkodous, A. S. Mahmoud, M. M. Rabee, A. H. Al-Muhtaseb and D. W. Rooney, *Environ. Chem. Lett.*, 2022, **20**, 519–562, DOI: 10.1007/s10311-021-01351-3.

22 I. Fatimah, G. Fadillah and S. P. Yudha, *Arab. J. Chem.*, 2021, **14**(8), 103301, DOI: 10.1016/j.arabjc.2021.103301.

23 F. Ozel, H. Kockar and O. Karaagac, *J. Supercond. Nov. Magn.*, 2015, **28**, 823–829, DOI: 10.1007/s10948-014-2707-9.

24 J. Li, X. Shi and M. Shen, *Part. Part. Syst. Charact.*, 2014, **31**(12), 1223–1237, DOI: 10.1002/ppsc.201400087.

25 M. M. Ba-Abbad, A. Benamour, D. Ewis, A. W. Mohammad and E. Mahmoudi, *JOM*, 2022, **74**, 3531–3539, DOI: 10.1007/s11837-022-05380-3.

26 M. Rashid, M. A. Rabbi, T. Ara, M. M. Hossain, M. S. Islam, A. Elaissari, H. Ahmad and M. M. Rahman, *RSC Adv.*, 2021, **11**, 36319–36328, DOI: 10.1039/D1RA04390K.

27 J. A. Fuentes-Garcia, A. C. Alavarse, A. C. M. Maldonado, A. Toro-Cordova, M. R. Ibarra and G. F. Goya, *ACS Omega*, 2020, **5**(41), 26357–26364, DOI: 10.1021/acsomega.0c02212.

28 M. Abbas, M. Takahashi, C. Kim and J. Nanopart, *J. Nanopart. Res.*, 2013, **15**, 1354.

29 A. Criveanu, F. Dumitrache, C. Fleaca, L. Gavrila-Florescu, I. Lungu, I. P. Morjan, V. Socoliuc and G. Prodan, *Appl. Surf. Sci. Adv.*, 2023, **15**, 100405, DOI: 10.1016/j.apsadv.2023.100405.

30 I. Morjan, R. Alexandrescu, F. Dumitrache, R. Birjega, C. Fleaca, I. Soare, C. R. Luculescu, G. Filoti, V. Kuncer and L. Vekas, *J. Nanosci. Nanotechnol.*, 2010, **10**, 1223–1234.

31 I. Karimzadeh, M. Aghazadeh, T. Doroudi, M. R. Ganjali and P. H. Kolivand, *Adv. Phys. Chem.*, 2017, 9437487, DOI: 10.1155/2017/9437487.

32 C. Pascal, J. L. Pascal, F. Favier, M. L. E. Moubtassim and C. Payen, *Chem. Mater.*, 1999, **11**(1), 141–147, DOI: 10.1021/cm980742f.

33 Y.-J. Liang, J. Xie, J. Yu, Z. Zheng, F. Liu and A. Yang, *Nano Select.*, 2021, **2**, 216–250, DOI: 10.1002/nano.202000169.

34 K. Vijayasri and A. Tiwari, *Inorg. Nano-Met. Chem.*, 2023, DOI: 10.1080/24701556.2023.2187418.

35 M. Aghayi-Anaraki and V. Safarifard, *Eur. J. Inorg. Chem.*, 2020, 1916–1937, DOI: 10.1002/ejic.202000012.

36 Q. Yang, Y. Dong, Y. Qiu, X. Yang, H. Cao and Y. Wu, *Colloids Surf. B*, 2020, **191**, 111014, DOI: 10.1016/j.colsurfb.2020.111014.

37 Q. Shen, B. Zhang, R. Xu, Y. Wang, X. Ding and P. Li, *Anaerobe*, 2010, **16**(4), 380–386.

38 M. R. Habib and M. R. Karim, *Micobiology*, 2009, **37**(1), 31–36.

39 J. Jalab, W. Abdelwahed, A. Kitaz and R. Al-Kayali, *Heliyon*, 2021, **7**(9), e08033, DOI: 10.1016/j.heliyon.2021.e08033.

40 A. M. Predescu, E. Matei, A. C. Berbecaru, C. Pantilimon, C. Drăgan, R. Vidu, C. Predescu and V. Kuncser, *Royal Soc. Open Sci.*, 2018, **5**(3), 171525, DOI: 10.1098/rsos.171525.

41 K. Parajuli, A. K. Sah and H. Paudyal, *Green Sustainable Chem.*, 2020, **10**, 117–132, DOI: 10.4236/gsc.2020.104009.

42 T. T. Nguyen, F. Mammeri, S. Ammar, T. B. N. Nguyen, T. N. Nguyen, T. H. L. Nghiem, N. T. Thuy and T. A. Ho, *Nanomaterials*, 2021, **11**, 1288, DOI: 10.3390/nano11051288.

43 S. S. U. Rahman, M. T. Qureshi, K. Sultana, W. Rehman, M. Y. Khan, M. H. Asif, M. Farooq and N. Sultana, *Results Phys.*, 2017, **7**, 4451–4456, DOI: 10.1016/j.rinp.2017.11.001.

44 J. Jeyasundari, P. S. Praba, Y. B. A. Jacob, V. S. Vasantha and V. Shanmugaiah, *Chem. Sci. Rev. Lett.*, 2017, **6**(22), 1244–1252.

45 S. Gil, E. Castro and J. F. Mano, *Mater. Lett.*, 2013, **100**, 266–270, DOI: 10.1016/j.matlet.2013.03.058.

46 A. Mukhopadhyay, N. Joshi, K. Chattopadhyay and G. De, *ACS Appl. Mater. Interfaces*, 2012, **4**, 142–149, DOI: 10.1021/am201166m.

47 K. Venugopal, H. A. Rather, K. Rajagopal, M. P. Shanthi, K. Sheriff, M. Illiyas, R. A. Rather, E. Manikandan, S. Uvarajan, M. Bhaskar and M. Maaza, *J. Photochem. Photobiol., B*, 2017, **167**, 282–289, DOI: 10.1016/j.jphotobiol.2016.12.013.

48 M. I. Majeed, J. Guo, W. Yan and B. Tan, *Polymers*, 2016, **8**, 392, DOI: 10.3390/polym8110392.

49 B. Maitra, M. H. Khatun, F. Ahmed, N. Ahmed, H. J. Kadri, M. Z. U. Rasel, B. K. Saha, M. Hakim, S. R. Kabir, M. R. Habib and M. A. Rabbi, *Arab. J. Chem.*, 2023, **16**(5), 104675, DOI: 10.1016/j.arabjc.2023.104675.

50 S. Lakshminarayanan, M. F. Shereen and K. L. Niraimathi, *et al.*, *Sci. Rep.*, 2021, **11**, 8643, DOI: 10.1038/s41598-021-87960-y.

51 K. Ssekatawa, D. K. Byarugaba, C. D. Kato, E. M. Wampande, F. Ejobi, J. L. Nakavuma, M. Maaza, J. Sackey, E. Nxumalo and J. B. Kirabira, *Front. Nanotechnol.*, 2021, **3**, 697303, DOI: 10.3389/fnano.2021.697303.

52 H. Alishah, S. P. Seyedi, S. Y. Ebrahimipour and S. Esmaeili-Mahani, *J. Clust. Sci.*, 2016, **27**, 421–429, DOI: 10.1007/s10876-016-0968-0.

53 B. L. Devi, K. M. Rao and D. Ramananda, *Appl. Phys. A.*, 2020, **126**, 924, DOI: 10.1007/s00339-020-04107-y.

54 S. Pirtarighat, M. Ghannadnia and S. Baghshahi, *J. Nanostructure Chem.*, 2019, **9**, 1–9, DOI: 10.1007/s40097-018-0291-4.

55 S. Monisha, T. Mathavan, S. Selvasekarapandian, A. M. F. Benial, G. Aristatil, N. Mani, M. Premalatha and D. V. Pandi, *Carbohydr. Polym.*, 2017, **157**, 38–47, DOI: 10.1016/j.carbpol.2016.09.026.

56 S. Sharmin, M. B. Islam, B. K. Saha, F. Ahmed, B. Maitra, M. Z. U. Rasel, N. Quaisaar and M. A. Rabbi, *Heliyon*, 2023, **9**, e20810, DOI: 10.1016/j.heliyon.2023.e20810.

57 L. M. Liz-Marzan, M. Giersig and P. Mulvaney, *Langmuir*, 1996, **12**(18), 4329–4335, DOI: 10.1021/la9601871.

58 J. Lim, S. P. Yeap, H. X. Che and S. C. Low, *Nanoscale Res. Lett.*, 2013, **8**(1), 381, DOI: 10.1186/1556-276X-8-381.

59 X.-F. Zhang, Z.-G. Liu, W. Shen and S. Gurunathan, *Int. J. Mol. Sci.*, 2016, **17**(9), 1534, DOI: 10.3390/ijms17091534.

60 B. Adebayo-Tayo, A. Salaam and A. Ajibade, *Heliyon*, 2019, **5**, e02502, DOI: 10.1016/j.heliyon.2019.e02502.

61 M. Almukainzi, *et al.*, *Int J Nanomedicine*, 2022, **17**, 1203–1225, DOI: 10.2147/IJN.S358606.

62 A. Tripathi, S. Kumari and A. Kumar, *Appl. Nanosci.*, 2016, **6**, 61–69, DOI: 10.1007/s13204-015-0414-x.

63 Y. Zhang, L. Cui, Y. Lu, J. He, H. Hussain, L. Xie, X. Sun, Z. Meng, G. Cao, D. Qin and D. Wang, *Thunb. Int. J. Nanomedicine*, 2023, **17**, 1647–1657, DOI: 10.2147/IJN.S356919.

64 A. K. Keshari, R. Srivastava, P. Singh, V. B. Yadav and G. Nath, *J. Ayurveda Integr. Med.*, 2020, **11**(1), 37–44, DOI: 10.1016/j.jaim.2017.11.003.

65 S. Salari, S. E. Bahabadi, A. Samzadeh-Kermani and F. Yosefzaei, *Iran J. Pharm. Res.*, 2019, **18**(1), 430–455.
66 M. A. Rabbi, M. M. Rahman, H. Minami, M. R. Habib and H. Ahmad, *Carbohydr. Polym.*, 2020, **233**, 115842, DOI: **10.1016/j.carbpol.2020.115842**.
67 R. Sharma, S. M. Jafari and S. Sharma, *Food Control*, 2020, **112**, 107086, DOI: **10.1016/j.foodcont.2020.107086**.
68 E. Karwowska, *Nanotechnol. Rev.*, 2017, **6**(2), 243–254, DOI: **10.1515/ntrev-2016-0046**.
69 S. Agnihotri, S. Mukherji and S. Mukherji, *Nanoscale*, 2013, **5**(16), 7328–7340, DOI: **10.1039/C3NR00024A**.

